JVST A
Journal of Vacuum Science & Technology A
ARTICLE
avs.scitation.org/journal/jva

Effect of crystallinity on thermal atomic layer etching of hafnium oxide, zirconium oxide, and hafnium zirconium oxide

Cite as: J. Vac. Sci. Technol. A **38**, 022608 (2020); doi: 10.1116/1.5135317
Submitted: 5 November 2019 · Accepted: 30 January 2020 ·
Published Online: 19 February 2020

View Online Export Citation CrossMark

Jessica A. Murdzek and Steven M. George

AFFILIATIONS

Department of Chemistry, University of Colorado, Boulder, Colorado 80309-0215

Note: This paper is part of the 2020 Special Topic Collection on Atomic Layer Etching (ALE).

ABSTRACT

Thermal atomic layer etching (ALE) can be achieved using sequential, self-limiting fluorination and ligand-exchange reactions. Previous studies have demonstrated thermal ALE of amorphous HfO_2 and ZrO_2 ALD films. This study explored the differences between thermal ALE of amorphous and polycrystalline films of hafnium oxide, zirconium oxide, and hafnium zirconium oxide on silicon wafers. HF, XeF_2, or SF_4 were used as the fluorination reactants. Titanium tetrachloride or dimethylaluminum chloride (DMAC) was employed as the metal precursor for ligand exchange. The spectroscopic ellipsometric measurements revealed that the amorphous films had much higher etch rates per cycle than the crystalline films regardless of the fluorination reactants or metal precursors for ligand exchange. The differences were most pronounced for HfO_2. Using HF and $TiCl_4$ as the reactants at 250 °C, the etch rates were 0.36 Å/cycle for amorphous HfO_2 and 0.02 Å/cycle for crystalline HfO_2. In comparison, the etch rates were 0.61 Å/cycle for amorphous ZrO_2 and 0.26 Å/cycle for crystalline ZrO_2. The etch rates were 0.35 Å/cycle for amorphous $HfZrO_4$ and 0.04 Å/cycle for crystalline $HfZrO_4$. When HF and DMAC were used as the reactants, the etch rates were higher than with HF and $TiCl_4$ for every material. Using HF and DMAC as the reactants at 250 °C, the etch rates were 0.68 Å/cycle for amorphous HfO_2 and 0.08 Å/cycle for crystalline HfO_2. In comparison, the etch rates were 1.11 Å/cycle for amorphous ZrO_2 and 0.82 Å/cycle for crystalline ZrO_2. The etch rates were 0.69 Å/cycle for amorphous $HfZrO_4$ and 0.16 Å/cycle for crystalline $HfZrO_4$. SF_4 as the fluorination reactant resulted in higher etch rates than for HF when using $TiCl_4$ as the metal precursor for ligand exchange. XeF_2 as the fluorination reactant resulted in even higher etch rates than for SF_4. The differences in the etch rate with the fluorination reactant can be partially attributed to differences in thermochemistry for fluorination by HF, SF_4, and XeF_2. The differences in etch rates between amorphous and crystalline films may be caused by the greater degree of fluorination and subsequent ligand-exchange reaction for the amorphous films. The amorphous films have a lower density and may be able to better accommodate the large volume expansion upon fluorination.

I. INTRODUCTION

Atomic layer etching (ALE) is a method used to remove thin films with Ångstrom-level precision using sequential, self-limiting surface reactions.[1] ALE can be accomplished with either plasma[1] or thermal[2,3] ALE methods. Plasma ALE yields anisotropic etching and involves a surface modification followed by an exposure of energetic ions or neutrals to remove material.[1,4] Thermal ALE yields isotropic etching and is viewed as the reverse of atomic layer deposition (ALD).[5–8] Like ALD, thermal ALE involves sequential exposures of gaseous reactants with inert gas purges in between the reactant exposures.[2,3]

Thermal ALE can be performed using fluorination and ligand-exchange reactions.[2,3] For metal oxides, the fluorination reaction converts the surface of the metal oxide to a surface fluoride layer. The ligand-exchange reaction can then volatilize the metal fluoride layer. In the ligand-exchange reaction, a metal precursor accepts a fluoride ligand from the metal fluoride surface and simultaneously donates one of its ligands to the metal fluoride surface. This step can produce stable and volatile metal products that can desorb from the surface.

Many metal oxides have been etched using thermal ALE with fluorination and ligand-exchange reactions including Al_2O_3, ZrO_2,

HfO_2, and VO_2.[2,9–11] Metal nitrides, such as AlN and GaN, can also be etched using fluorination and ligand-exchange reactions.[12,13] Other mechanisms for thermal ALE are also possible including oxidation and fluorination to a volatile fluoride. This mechanism has been demonstrated for TiN ALE.[14] Thermal ALE can also be accomplished using conversion reactions where the original substrate material is converted to a different material. Conversion mechanisms have been employed for SiO_2 and ZnO ALE.[15,16] Likewise, oxidation and conversion mechanisms can be combined for W and Si ALE.[17,18]

Thermal ALE of amorphous HfO_2 and ZrO_2 has been performed using fluorination and ligand-exchange reactions. HF has been used for fluorination, and $Sn(acac)_2$, $AlCl(CH_3)_2$ [dimethylaluminum chloride (DMAC)], or $TiCl_4$ have been used as the metal precursors for ligand exchange.[7,10,19,20] Fluorination and ligand-exchange reactions for HfO_2 ALE using HF and $TiCl_4$ are illustrated in Fig. 1.[20] In contrast, there have been no reports for thermal ALE of crystalline ZrO_2 and HfO_2. Other crystalline materials, such as AlN, have been etched using thermal ALE.[12] Crystalline AlN has been etched using HF for fluorination and $Sn(acac)_2$ as the metal precursor for ligand exchange.[12] There have been no reports for thermal ALE of amorphous AlN.

One possible application for thermal ALE of crystalline materials is the thinning of metal oxides used as gate oxides in advanced gate stacks. HfO_2 and ZrO_2 both have high dielectric constants that facilitate their use as gate oxides.[21,22] Crystalline HfO_2 and ZrO_2 in their cubic and tetragonal phases have higher dielectric constants than their amorphous counterparts.[23,24] The higher dielectric constant aids the use of crystalline HfO_2 and ZrO_2 in advanced gate stacks.

The etching of crystalline HfO_2 and ZrO_2 films is important because etching provides a pathway to obtain ultrathin crystalline films. The crystallization temperature typically increases as the film thickness decreases. For example, the crystallization temperature increased from 425 to 600 °C as the HfO_2 film thickness was decreased from 40 to 5 nm, respectively, for HfO_2 ALD films deposited at 300 °C.[25] Preferential crystallization for thicker films was also observed for HfO_2 films prepared using ion-assisted deposition,[26] HfSiON films grown by ALD,[27] and Si-doped HfO_2 films deposited by ALD.[28] The reduction of the crystallization temperature for thicker films can be explained by their lower surface-to-volume ratios that favor their crystalline phases.[26,28,29]

The crystallization temperatures of amorphous HfO_2 and ZrO_2 are approximately 475–600 °C and 425–500 °C, respectively.[29,30] The crystallization temperatures also increase as a function of dopant concentration in HfO_2 and ZrO_2.[29,30] In addition, thinner films crystallize at higher temperatures than thicker films as discussed above.[25] Consequently, when there are temperature constraints, amorphous HfO_2 and ZrO_2 films may have to be grown thicker, crystallized, and then etched back to obtain the desired ultrathin crystalline thickness.[3] A schematic illustrating this ALD and ALE processing sequence is shown in Fig. 2.

Differences between thermal ALE of amorphous and crystalline films may also be important for selective ALE. Selectivity is obtained when two different materials have different etch rates under the same conditions or when one material etches while the other does not etch.[10] Selective thermal ALE has been observed for a variety of metal precursors and materials.[10,14] Selectivity could also be observed between amorphous and crystalline phases of the same material. For example, crystalline films may etch slower than amorphous films. After a low temperature anneal, thinner films that only crystallize at higher temperatures could be etched preferentially to thicker films that crystallize at lower temperatures.

There are many examples of etching differences between amorphous and crystalline materials in the literature. For example, amorphous silicon-based alloys display much higher etch rates than crystalline silicon-based alloys during etching with gas phase HCl.[31] Hydrogenated amorphous silicon also displays selective etching with respect to crystalline silicon during etching with hydrogen plasma.[32] Amorphous SiC is also etched much faster than crystalline SiC by CF_4/O_2 plasma exposures.[33] Amorphous HfO_2 is etched much faster during wet HF etching than crystalline HfO_2.[34] In addition, various phase-change materials display much higher etching rates for the material in the amorphous state

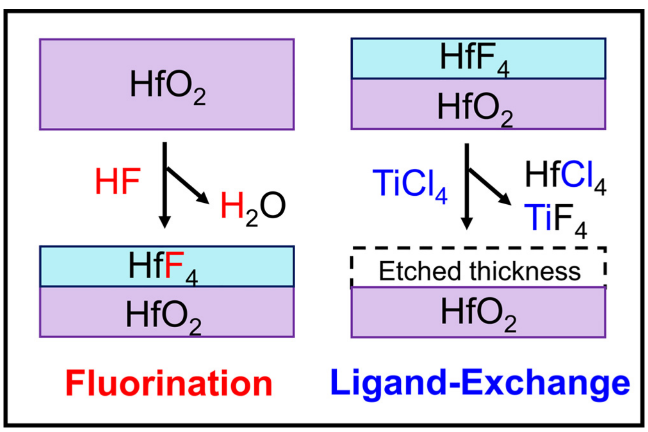

FIG. 1. Schematic for HfO_2 ALE using HF and $TiCl_4$ as the reactants in the fluorination and ligand-exchange reactions, respectively.

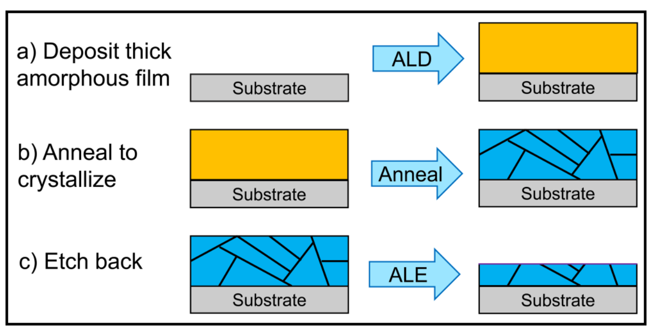

FIG. 2. Schematic detailing a processing sequence to produce an ultrathin crystalline film based on (a) ALD of a thick amorphous film, (b) annealing to crystallize the thick amorphous film, and (c) etching back the thick crystalline film to obtain an ultrathin crystalline film.

compared with the crystalline state.[35–38] Amorphous polymers are also known to etch more rapidly than crystalline polymers.[39,40]

In this study, fluorination and ligand-exchange reactions were used to etch amorphous and crystalline HfO_2, ZrO_2, and $HfZrO_4$ films on silicon wafers. A preliminary version of some of this investigation appeared in the extended abstract for the *VLSI-TSA 2019 Symposium*.[41] The fluorination reagents were HF, SF_4, and XeF_2. The metal precursors for the ligand-exchange reaction were DMAC and $TiCl_4$. The comparison between the etch rates of amorphous and crystalline HfO_2, ZrO_2, and $HfZrO_4$ was performed at 250 °C. Film thickness measurements were performed as a function of the number of ALE cycles using *ex situ* spectroscopic ellipsometry (SE) measurements. Changes in film thickness versus the number of ALE cycles were used to determine the etch rates.

II. EXPERIMENT

Thermal ALE experiments were performed in a viscous flow reactor.[42] The reaction temperatures were maintained by a proportional-integral-derivative temperature controller (2604, Eurotherm). A constant flow of ultrahigh purity N_2 gas was employed as the carrier and purge gas using mass flow controllers (type 1179A, MKS). A mechanical pump (Pascal 2015SD, Alcatel) was attached at the back of the reactor. The reactor pressure with flowing N_2 carrier gas was 1 Torr. This pressure was measured by a capacitance manometer (Baratron 121A, MKS).

The fluorination reactions used either HF-pyridine solution (70 wt. % HF, Sigma-Aldrich), SF_4 (>98.5%, SynQuest Laboratories), or XeF_2 (99.5%, Strem Chemicals). The fluorination agents were maintained at room temperature. The HF-pyridine solution was contained in a gold-plated stainless steel bubbler to prevent corrosion. The pressure transients of HF from the HF-pyridine source were adjusted to ∼90 mTorr using a metering valve (SS-4BMG, Swagelok). The SF_4 pressure transients were ∼200 mTorr using a metering valve. The XeF_2 pressure transients were ∼10 mTorr without a metering valve. The ligand-exchange precursors were titanium tetrachloride, $TiCl_4$ (99.9% Sigma-Aldrich) and DMAC (97%, Sigma-Aldrich). Both $TiCl_4$ and DMAC were held at room temperature. Metering valves were used to maintain pressure transients of ∼40 mTorr for DMAC and ∼100 mTorr for $TiCl_4$.

This work employed ZrO_2, HfO_2, and $HfZrO_4$ thin films on silicon wafers provided by TEL Technology Center, America, LLC. The films were deposited using ALD methods at 250 °C on a chemical oxide with a thickness of ∼10 Å on silicon wafers. Most of the ZrO_2, HfO_2, and $HfZrO_4$ films had a thickness of approximately 100 Å. The as-deposited, amorphous films were used without further modification. The crystalline films were annealed using the cyclical deposition-anneal-deposition-anneal process.[43–46] The annealing was conducted at 800 °C for 40 s in an N_2 environment.[46] These crystalline films are reported to be fiber-textured.[46]

Figure 3 shows the grazing incidence x-ray diffraction scan for each of the crystalline HfO_2, ZrO_2, and $HfZrO_4$ films. The crystalline ZrO_2 film was tetragonal.[47] The crystalline HfO_2 film was monoclinic.[48] The crystalline $HfZrO_4$ film was a mixture of monoclinic and tetragonal phases. This mixture of different crystal phases has been previously observed in $HfZrO_4$.[49,50]

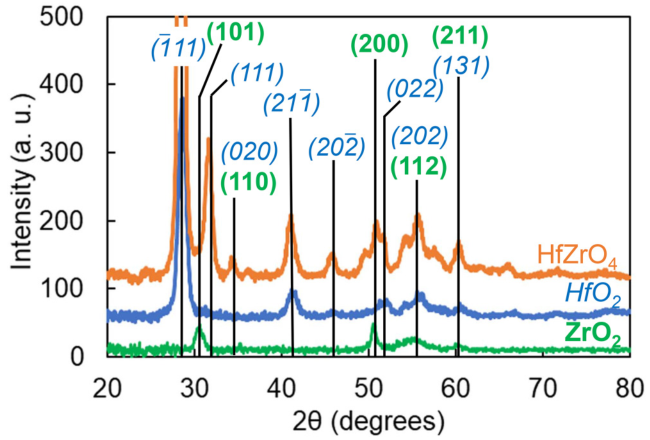

FIG. 3. XRD scans for the crystalline HfO_2, ZrO_2, and $HfZrO_4$ films. The italicized labels correspond to monoclinic HfO_2 peaks. The bold labels correspond to tetragonal ZrO_2 peaks. The HfO_2 and ZrO_2 films had a thickness of 100 Å. The $HfZrO_4$ films had a thickness of 250 Å.

The wafers were cut into pieces that were each $2 \times 2\ cm^2$ in size. For each experiment, one of each material and morphology was placed in the reactor. Six total samples were included in each experiment to allow for comparisons between the materials and morphologies.

ALE experiments were performed with a reaction sequence of x-30-2-30. This signifies a fluorination reactant exposure of x seconds, then a 30 s N_2 purge, subsequently a 2 s exposure of the metal precursor, and then another 30 s N_2 purge. Experiments using HF had a reaction sequence of 1-30-2-30. These conditions were in the self-limiting, saturation regime using HF as the fluorination reactant and $TiCl_4$ and DMAC as the metal precursors for ALE of the amorphous films.[7,20] Additional experiments confirmed that the etch rates for the crystalline films were not increased using higher pressures for the metal precursors. Experiments using SF_4 had a reaction sequence of 1-30-2-30. The reaction sequence was 3-30-2-30 when using XeF_2 as the fluorination reactant.

The film thicknesses were measured using *ex situ* SE measurements. The spectroscopic ellipsometer (M-2000, J. A. Woollam) measured Ψ and Δ from 240 to 1000 nm with an incidence angle of 70°. CompleteEASE software was used to model the data to determine the thickness and optical constants, n (refractive index) and k (extinction coefficient). The etch rate was determined using film thickness measurements over many ALE cycles.

The precision of the SE measurements of film thickness was within ±0.05 Å. A Cauchy model was used to model the SE data for all the films. The etch rates obtained from individual ALE experiments using HF and XeF_2 as the fluorination reactants were accurate to ±0.04 Å/cycle. The reproducibility of the etch rates as determined from repeated experiments under the same conditions was ±0.05 Å/cycle. ALE experiments that used SF_4 as the fluorination reactant had a slightly higher variability. The reason for the larger data scattering when using SF_4 is not known.

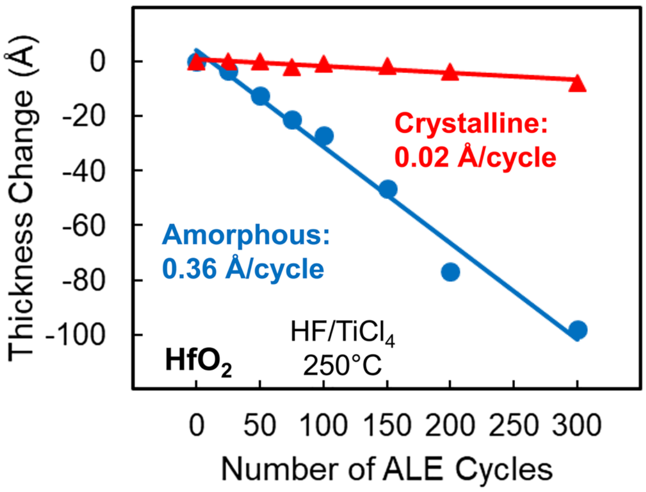

FIG. 4. Thickness change vs number of ALE cycles for the amorphous and crystalline HfO_2 films using HF and $TiCl_4$ as the reactants at 250 °C.

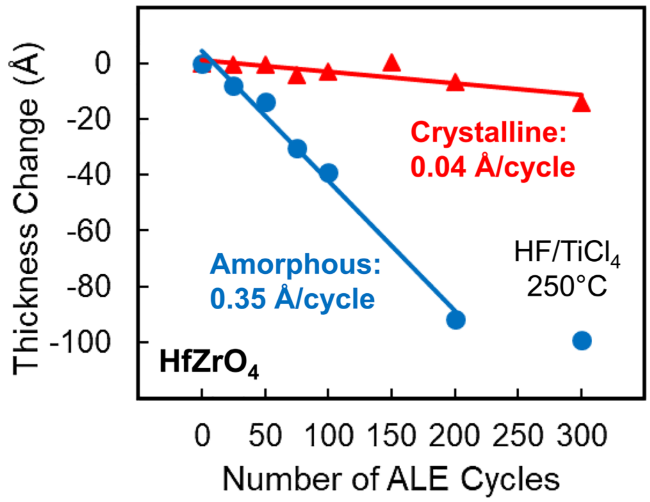

FIG. 6. Thickness change vs number of ALE cycles for the amorphous and crystalline $HfZrO_4$ films using HF and $TiCl_4$ as the reactants at 250 °C.

III. RESULTS AND DISCUSSION

Large differences between the etch rates for amorphous and crystalline materials were observed using HF and $TiCl_4$ as the reactants at 250 °C. Figure 4 shows the thickness change versus the number of ALE cycles for HfO_2. The etch rate for the amorphous HfO_2 film was 0.36 Å/cycle. For the crystalline HfO_2 film, the etch rate was 0.02 Å/cycle. The etch rate of the amorphous HfO_2 film was 18 times higher than the etch rate for crystalline HfO_2 films.

Figure 5 displays the results for the ZrO_2 films using HF and $TiCl_4$ as the reactants at 250 °C. The amorphous ZrO_2 film had an etch rate of 0.61 Å/cycle. For the crystalline ZrO_2 film, the etch rate was 0.26 Å/cycle. The amorphous ZrO_2 film was completely removed after 150 cycles.

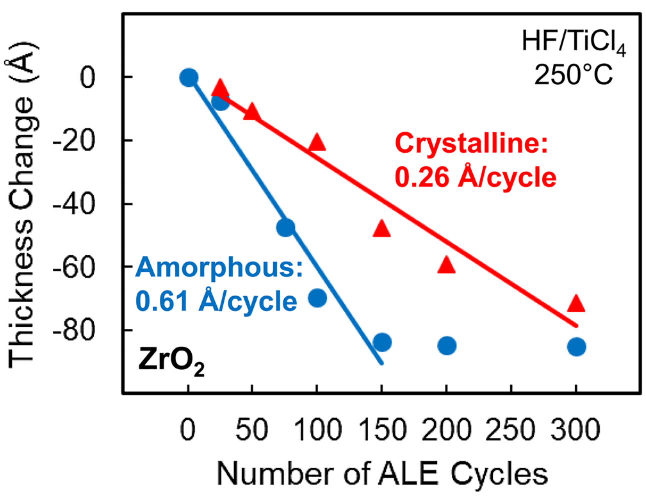

FIG. 5. Thickness change vs number of ALE cycles for the amorphous and crystalline ZrO_2 films using HF and $TiCl_4$ as the reactants at 250 °C.

Figure 6 shows the etching results for the $HfZrO_4$ films using HF and $TiCl_4$ as the reactants at 250 °C. The etch rate for the amorphous $HfZrO_4$ film was 0.35 Å/cycle. This amorphous $HfZrO_2$ film was completely removed in about 200 ALE cycles. In contrast, the etch rate for the crystalline $HfZrO_4$ film was 0.04 Å/cycle.

Figures 4–6 illustrate that the amorphous films had higher etch rates than their crystalline counterparts for HfO_2, ZrO_2, and $HfZrO_4$ using HF and $TiCl_4$ as the reactants. The etch rates for HF and $TiCl_4$ as the reactants at 250 °C are listed in Table I.

Other metal precursors can also undergo ligand exchange with hafnium, zirconium, and hafnium zirconium fluorides and produce ALE. DMAC is a versatile precursor for ligand exchange. Figure 7 shows the results for HfO_2 etching using HF and DMAC as the reactants at 250 °C. The amorphous HfO_2 film had an etch rate of 0.68 Å/cycle. This amorphous HfO_2 film was completely removed after 150 cycles. In contrast, the crystalline HfO_2 film had a much lower etch rates of 0.08 Å/cycle.

Figure 8 displays the results for etching the ZrO_2 films using HF and DMAC at 250 °C. In contrast to the previous results using HF and $TiCl_4$ as the reactants, both ZrO_2 films display a fairly high etch per cycle. The etch rates were 1.11 and 0.82 Å/cycle for the amorphous and crystalline films, respectively. The amorphous ZrO_2 film was completely etched away after 75 cycles. The crystalline ZrO_2 film was completely etched away after 100 cycles.

Figure 9 shows the results for etching the $HfZrO_4$ films using HF and DMAC at 250 °C. The amorphous $HfZrO_4$ film had an etch rate of 0.69 Å/cycle. The amorphous $HfZrO_4$ film was etched completely in 150 ALE cycles. In contrast, the etch rates for the crystalline $HfZrO_4$ film was 0.16 Å/cycle.

TABLE I. Etch rates in Å/cycle using different fluorination reactants and metal precursors for ligand exchange at 250 °C for amorphous and crystalline HfO_2, ZrO_2, and $HfZrO_4$ films.

Fluorination agent	Ligand-exchange agent	Amorphous HfO_2	Crystalline HfO_2	Amorphous ZrO_2	Crystalline ZrO_2	Amorphous $HfZrO_4$	Crystalline $HfZrO_4$
HF	$TiCl_4$	0.36	0.02	0.61	0.26	0.35	0.04
HF	DMAC	0.68	0.08	1.11	0.82	0.69	0.16
SF_4	$TiCl_4$	0.70	0.08	1.08	0.36	0.62	0.25
SF_4	DMAC	0.50	No etch	0.46	0.34	0.49	No etch
XeF_2	$TiCl_4$	1.96	1.26	2.69	1.75	2.07	1.71

In similarity with the etch rates using HF and $TiCl_4$ as the reactants, the etch rates for HfO_2, ZrO_2, and $HfZrO_4$ using HF and DMAC as the reactants are much slower for the crystalline films. However, using DMAC in place of $TiCl_4$ with HF results in higher etch rates. The etch rates for HF and DMAC as the reactants at 250 °C are given in Table I.

There are dramatic differences between ALE of amorphous and crystalline materials. Amorphous materials have a lower density than crystalline materials. The lower density may facilitate fluorination because fluorination leads to the expansion of the metal oxide. For example, the molar volume of crystalline HfO_2 is 210.49 g/mol/9.68 g/cm^3 = 21.745 cm^3/mol. In contrast, the molar volume of crystalline HfF_4 is 254.48 g/mol/7.1 g/cm^3 = 35.84 cm^3/mol. The volume expansion upon fluorination of HfO_2 to HfF_4 is 1.65. Likewise, the molar volume of crystalline ZrO_2 is 123.218 g/mol/5.68 g/cm^3 = 21.693 cm^3/mol. In contrast, the molar volume of crystalline ZrF_4 is 167.21 g/mol/4.43 g/cm^3 = 37.745 cm^3/mol. The volume expansion upon fluorination of ZrO_2 to ZrF_4 is 1.74.

The lower density of the amorphous materials may also allow for an easier replacement of oxygen with fluorine during fluorination. Previous studies have also shown that there are oxygen vacancies in the amorphous structures of HfO_2 and ZrO_2.[51–53] These oxygen vacancies may help facilitate fluorine diffusion deeper into the amorphous structure. The resulting thicker fluoride layer may then lead to more fluoride removed during the ligand-exchange reaction.[54]

The higher density crystalline materials also have bond lengths and configurations that are more uniform than for amorphous materials. The crystalline structures will also have fewer oxygen vacancies. Fewer oxygen vacancies may result in less fluorine diffusion and a thinner fluoride layer. The thinner fluoride layer would lead to a lower etch rate.[54] On the other hand, crystalline materials may have grain boundaries that could affect etching. The lower etch rate for the crystalline materials argues that the possible enhancement effect of grain boundaries is minimal.

Other fluorination reactants are also effective for thermal ALE. SF_4 and XeF_2 are both stronger fluorination reactants than HF. Thermochemical calculations at 250 °C show that fluorination of HfO_2 and ZrO_2 with SF_4 is more favorable than fluorination with HF. The standard free energies for fluorination of HfO_2 by HF and SF_4 at 250 °C are $\Delta G° = -16$ and -85 kcal, respectively.[55] The standard free energies for fluorination of ZrO_2 by HF and

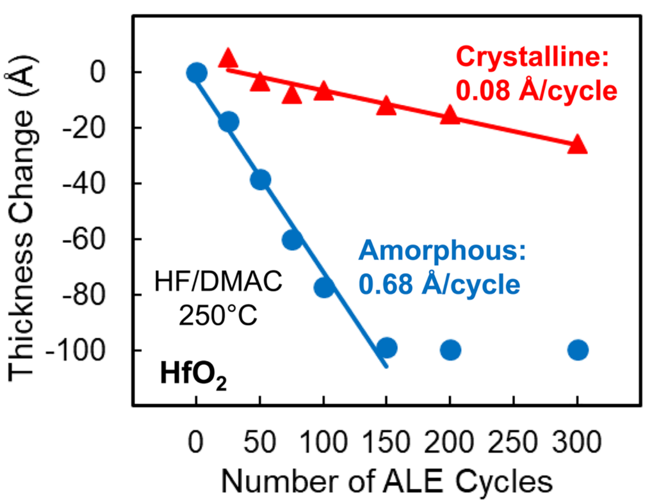

FIG. 7. Thickness change vs number of ALE cycles for the amorphous and crystalline HfO_2 films using HF and DMAC as the reactants at 250 °C.

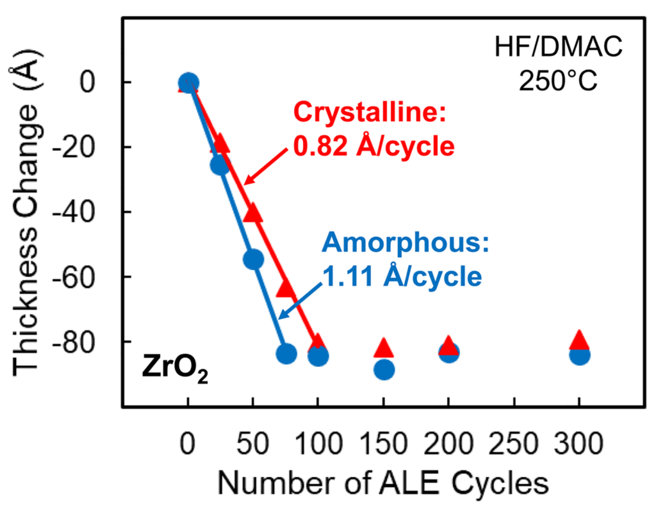

FIG. 8. Thickness change vs number of ALE cycles for the amorphous and crystalline ZrO_2 films using HF and DMAC as the reactants at 250 °C.

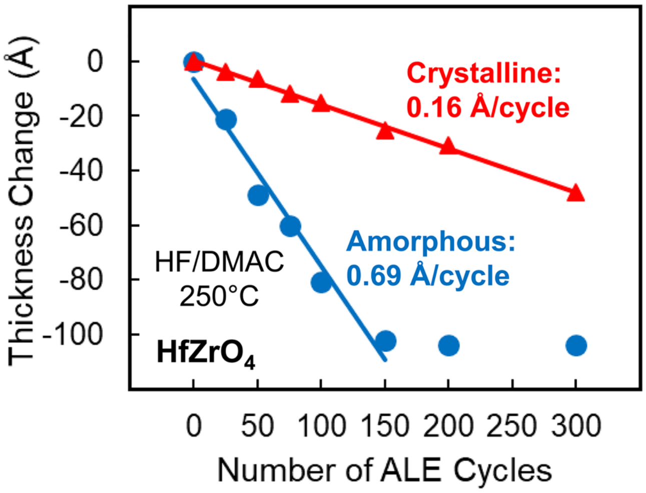

FIG. 9. Thickness change vs number of ALE cycles for the amorphous and crystalline $HfZrO_4$ films using HF and DMAC as the reactants at 250 °C.

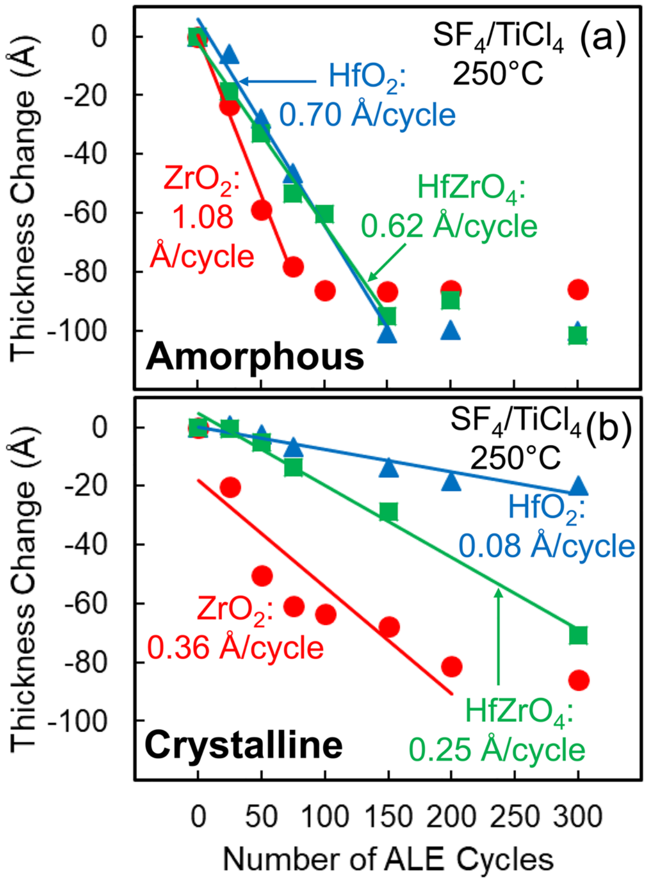

FIG. 10. Thickness change vs number of ALE cycles for (a) amorphous and (b) crystalline films of HfO_2, ZrO_2, and $HfZrO_4$ using SF_4 and $TiCl_4$ as the reactants at 250 °C.

SF_4 at 250 °C are $\Delta G° = -15$ and -84 kcal, respectively.[55] Based on these thermochemical calculations, SF_4 is a promising fluorination reactant.

Figure 10(a) shows the etch results using SF_4 and $TiCl_4$ for amorphous HfO_2, $HfZrO_4$, and ZrO_2 films at 250 °C. The etch rates were 0.70, 0.62, and 1.08 Å/cycle, respectively. All the amorphous materials have reasonably high etch rates. Figure 10(b) shows the etch results using SF_4 and $TiCl_4$ for the HfO_2, $HfZrO_4$, and ZrO_2 crystalline films. The etch rates were 0.08, 0.25, and 0.36 Å/cycle, respectively. In similarity to the etching of the crystalline films using HF and $TiCl_4$, ZrO_2 has the highest etch rate, HfO_2 has the lowest etch rate, and $HfZrO_4$ has an etch rate that is between the ZrO_2 and HfO_2 etch rates. The etch rates using the SF_4 and $TiCl_4$ reactants were also higher than the etch rates using the HF and $TiCl_4$ reactants. These higher etch rates for SF_4 can be attributed to the larger $-\Delta G°$ values for fluorination using SF_4. The etch rates for SF_4 and $TiCl_4$ as the reactants at 250 °C are given in Table I.

SF_4 and DMAC were also used as the reactants at 250 °C to etch the various metal oxide materials. For amorphous HfO_2, $HfZrO_4$, and ZrO_2, the etch rates were 0.50, 0.49, and 0.46 Å/cycle, respectively. These etch rates are not significantly different from each other. No etching was observed for the HfO_2 and $HfZrO_4$ crystalline materials using SF_4 and DMAC. The lack of etching for crystalline HfO_2 and $HfZrO_4$ using SF_4 and DMAC as the reactants is not understood at this time. In contrast, the crystalline ZrO_2 film had an etch rate of 0.34 Å/cycle. When compared with the etch rates using SF_4 and $TiCl_4$ as the reactants, SF_4 and DMAC as the reactants decrease the etch rates of all the metal oxide materials. The etch rates for SF_4 and DMAC as the reactants at 250 °C are provided in Table I.

XeF_2 is an even stronger fluorination reactant than SF_4. For the reactions $MO_2 + 2XeF_2(g) \rightarrow MF_4 + O_2(g) + 2Xe(g)$, the standard free energies for fluorination of HfO_2 and ZrO_2 at 250 °C are $\Delta G° = -153$ and -153 kcal, respectively.[55] Figure 11(a) shows the etching results using XeF_2 and $TiCl_4$ as the reactants at 250 °C for amorphous HfO_2, ZrO_2, and $HfZrO_4$. ZrO_2 had the highest etch rate of 2.69 Å/cycle. HfO_2 had the smallest etch rate of 1.96 Å/cycle. $HfZrO_4$ had an etch rate of 2.07 Å/cycle that was between ZrO_2 and HfO_2. These etch rates are all higher than the etch rates using SF_4 and $TiCl_4$ as the reactants. These high etch rates are attributed to larger $-\Delta G°$ values for fluorination by XeF_2.

The etch results for the crystalline films using XeF_2 and $TiCl_4$ as the reactants are shown in Fig. 11(b). The etch rates for the HfO_2, $HfZrO_4$, and ZrO_2 crystalline films were 1.26, 1.71, and 1.75 Å/cycle, respectively. The etch rates for the crystalline films are smaller than the etch rates for the corresponding amorphous films. However, the etch rates are considerably larger than the etch rates using HF and $TiCl_4$ or SF_4 and $TiCl_4$ as the reactants. Crystalline HfO_2 can be etched successfully using XeF_2 and $TiCl_4$ as the reactants at 250 °C. The etch rates for XeF_2 and $TiCl_4$ as the reactants at 250 °C are given in Table I.

One potential problem with XeF_2 is that XeF_2 is known to spontaneously etch silicon.[56] Additionally, a proximity effect has

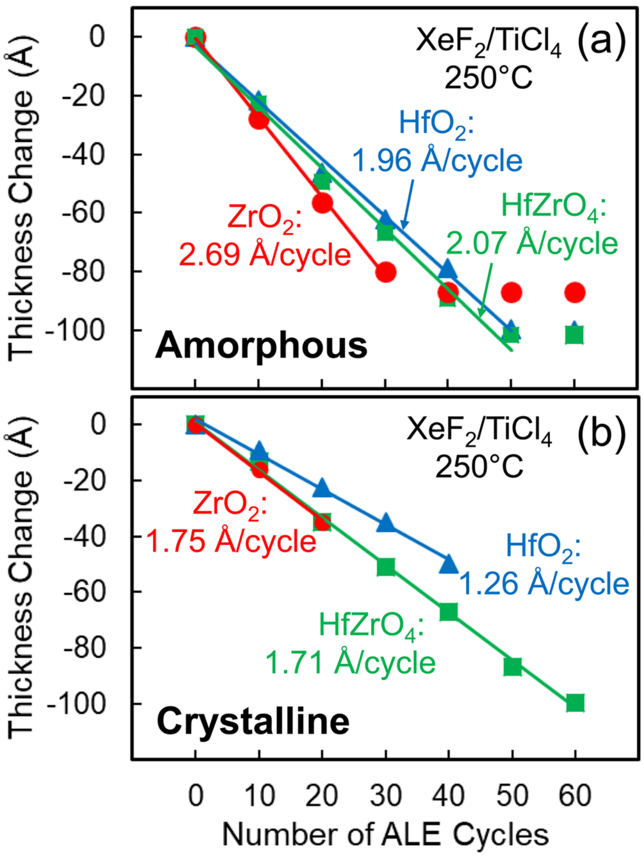

FIG. 11. Thickness change vs number of ALE cycles for (a) amorphous and (b) crystalline films of HfO_2, ZrO_2, and $HfZrO_4$ using XeF_2 and $TiCl_4$ as the reactants at 250 °C.

been observed that resulted in a spontaneous etch of SiO_2 in the presence of Si using XeF_2.[57] The materials used in this study were grown on the native oxide of a silicon wafer. To determine if there was spontaneous etching by XeF_2, each material was subjected to multiple doses of XeF_2 at 250 °C. After 30 consecutive XeF_2 doses for 3 s, a small thickness loss was observed after about five XeF_2 doses. The thickness loss was between 5 and 10 Å. However, continued XeF_2 doses did not result in any further thickness change. These results rule out any spontaneous etching of HfO_2, ZrO_2, or $HfZrO_4$ by XeF_2 at 250 °C.

The larger etch rates for XeF_2 compared with SF_4 are expected based on the ΔG° values for fluorination. For example, the standard free energy changes for fluorination of HfO_2 by either SF_4 or XeF_2 at 250 °C are $\Delta G° = -85$ and -153 kcal, respectively.[55] Additional differences may result from the different nature of the SF_4 and XeF_2 fluorination reactants. SF_4 is a nucleophilic fluorination reactant, and SF_4 acts as an F^- donor. In contrast, XeF_2 is an electrophilic fluorination reactant and F in XeF_2 acts as an electron acceptor. The fluorine radicals released by XeF_2 may be able to penetrate further into the metal oxide film. The possibly thicker fluoride layer resulting from the F radicals from XeF_2 may lead to more ligand-exchange reactions and higher etch rates.[54]

IV. CONCLUSIONS

Thermal HfO_2, ZrO_2, and $HfZrO_4$ ALE can be accomplished using fluorination and ligand-exchange reactions with HF, SF_4, or XeF_2 as the fluorination reactants and $TiCl_4$ or DMAC as the metal precursors for ligand exchange. This study examined the differences between thermal ALE for amorphous and crystalline films at 250 °C. The etch rates for the amorphous metal oxides were significantly higher than the etch rates for the crystalline metal oxides. Under a given set of reaction conditions, ZrO_2 films had the highest etch rates and HfO_2 films had the lowest etch rates. The majority of the etch rates for $HfZrO_4$ films were in between ZrO_2 and HfO_2 films.

Etching rates were measured at 250 °C using the following pairs of fluorination reactant/metal precursor: HF/$TiCl_4$, HF/DMAC, SF_4/$TiCl_4$, SF_4/DMAC, and XeF_2/$TiCl_4$. Using $TiCl_4$ as the metal precursor for ligand exchange, the etch rates increased with the fluorination reactant according to the following ordering: $HF < SF_4 < XeF_2$ for all the amorphous and crystalline films. The etch rates increased in correspondence with the standard free energies of fluorination for HF, SF_4, and XeF_2.

The best etch selectivity between amorphous and crystalline structures was observed for HfO_2. Using HF and $TiCl_4$ as the reactants at 250 °C, the etch rates were 0.36 Å/cycle for amorphous HfO_2 and 0.02 Å/cycle for crystalline HfO_2. The most comparable etching rates between amorphous and crystalline structures were observed for ZrO_2. Using HF and DMAC as the reactants at 250 °C, the etch rates were 1.11 Å/cycle for amorphous ZrO_2 and 0.82 Å/cycle for crystalline ZrO_2. The largest etch rates for the crystalline films were observed using XeF_2 as the fluorination reactant. Using XeF_2 and $TiCl_4$ as the reactants at 250 °C, the etch rates were 1.26 Å/cycle for crystalline HfO_2, 1.75 Å/cycle for crystalline ZrO_2, and 1.71 Å/cycle for crystalline $HfZrO_4$.

The differences between the etching rates of amorphous and crystalline films are attributed to their different densities and structures. Amorphous materials have a lower density than crystalline materials. The lower density may facilitate fluorination because fluorination leads to a significant molar volume expansion. The lower density may also allow for an easier replacement of oxygen with fluorine during fluorination. A thicker fluoride film after fluorination will lead to more fluoride removed during the ligand-exchange reaction and larger etch rates. The more ordered structure of the crystalline films also has fewer vacancies and defects than the amorphous films. These vacancies and defects may facilitate the fluorination and ligand-exchange reactions during thermal ALE.

ACKNOWLEDGMENTS

This research was funded by the National Science Foundation (NSF) (No. CHE-1609554). The authors thank Kanda Tapily and Gert Leusink from the TEL Technology Center, America, LLC, for providing the HfO_2, ZrO_2, and $HfZrO_4$ samples. The authors also thank Andrew Kummel at the University of California at San Diego for valuable discussions.

REFERENCES

[1]K. J. Kanarik, T. Lill, E. A. Hudson, S. Sriraman, S. Tan, J. Marks, V. Vahedi, and R. A. Gottscho, J. Vac. Sci. Technol. A **33**, 020802 (2015).
[2]Y. Lee and S. M. George, ACS Nano **9**, 2061 (2015).
[3]S. M. George and Y. Lee, ACS Nano **10**, 4889 (2016).
[4]C. T. Carver, J. J. Plombon, P. E. Romero, S. Suri, T. A. Tronic, and R. B. Turkot, ECS J. Solid State Sci. Technol. **4**, N5005 (2015).
[5]T. Faraz, F. Roozeboom, H. C. M. Knoops, and W. M. M. Kessels, ECS J. Solid State Sci. Technol. **4**, N5023 (2015).
[6]S. M. George, Chem. Rev. **110**, 111 (2010).
[7]Y. Lee and S. M. George, J. Phys. Chem. C **123**, 18455 (2019).
[8]D. R. Zywotko, J. Faguet, and S. M. George, J. Vac. Sci. Technol. A **36**, 061508 (2018).
[9]Y. Lee, J. W. DuMont, and S. M. George, Chem. Mater. **27**, 3648 (2015).
[10]Y. Lee, C. Huffman, and S. M. George, Chem. Mater. **28**, 7657 (2016).
[11]J. C. Gertsch, A. M. Cano, V. M. Bright, and S. M. George, Chem. Mater. **31**, 3624 (2019).
[12]N. R. Johnson, H. Sun, K. Sharma, and S. M. George, J. Vac. Sci. Technol. A **34**, 050603 (2016).
[13]N. R. Johnson, J. K. Hite, M. A. Mastro, C. R. Eddy, and S. M. George, Appl. Phys. Lett. **114**, 243103 (2019).
[14]Y. Lee and S. M. George, Chem. Mater. **29**, 8202 (2017).
[15]J. W. DuMont, A. E. Marquardt, A. M. Cano, and S. M. George, ACS Appl. Mater. Interfaces **9**, 10296 (2017).
[16]D. R. Zywotko and S. M. George, Chem. Mater. **29**, 1183 (2017).
[17]A. I. Abdulagatov and S. M. George, Chem. Mater. **30**, 8465 (2018).
[18]N. R. Johnson and S. M. George, ACS Appl. Mater. Interfaces **9**, 34435 (2017).
[19]Y. Lee, J. W. DuMont, and S. M. George, ECS J. Solid State Sci. Technol. **4**, N5013 (2015).
[20]Y. Lee and S. M. George, J. Vac. Sci. Technol. A **36**, 061504 (2018).
[21]A. Ghetti *et al.*, Microelectron. Reliab. **40**, 557 (2000).
[22]J. Robertson, Eur. Phys. J. Appl. Phys. **28**, 265 (2004).
[23]D. Ceresoli and D. Vanderbilt, Phys. Rev. B **74**, 125108 (2006).
[24]D. Vanderbilt, X. Y. Zhao, and D. Ceresoli, Thin Solid Films **486**, 125 (2005).
[25]E. P. Gusev, C. Cabral, M. Copel, C. D'Emic, and M. Gribelyuk, Microelectron. Eng. **69**, 145 (2003).
[26]L. Zhang, J. L. Zhang, H. F. Jiao, G. H. Bao, Z. S. Wang, and X. B. Cheng, Thin Solid Films **642**, 359 (2017).
[27]G. Pant, A. Gnade, M. J. Kim, R. M. Wallace, B. E. Gnade, M. A. Quevedo-Lopez, and P. D. Kirsch, Appl. Phys. Lett. **88**, 032901 (2006).
[28]E. Yurchuk, J. Muller, S. Knebel, J. Sundqvist, A. P. Graham, T. Melde, U. Schroder, and T. Mikolajick, Thin Solid Films **533**, 88 (2013).
[29]S. V. Ushakov *et al.*, Phys. Status Solidi B **241**, 2268 (2004).
[30]S. V. Ushakov, C. E. Brown, and A. Navrotsky, J. Mater. Res. **19**, 693 (2004).
[31]M. Bauer and S. G. Thomas, Thin Solid Films **520**, 3139 (2012).
[32]M. Otobe, M. Kimura, and S. Oda, Jpn. J. Appl. Phys. **33**, 4442 (1994).
[33]R. Padiyath, R. L. Wright, M. I. Chaudhry, and S. V. Babu, Appl. Phys. Lett. **58**, 1053 (1991).
[34]J. H. Chen, W. J. Yoo, and D. S. H. Chan, J. Electrochem. Soc. **153**, G483 (2006).
[35]C. H. Chu, C. D. Chiun, H. W. Cheng, M. L. Tseng, H. P. Chiang, M. Mansuripur, and D. P. Tsai, Opt. Express **18**, 18383 (2010).
[36]T. Luo, Z. Li, Q. He, and X. S. Miao, Opt. Express **24**, 5754 (2016).
[37]B. J. Zeng, J. Z. Huang, R. W. Ni, N. N. Yu, W. Wei, Y. Z. Hu, Z. Li, and X. S. Miao, Sci. Rep. **4**, 5300 (2014).
[38]K. Zhang, Z. W. Wang, G. D. Chen, Y. Wang, A. J. Zeng, J. Zhu, S. Avakaw, and H. Tsikhanchuk, Chin. Opt. Lett. **17**, 093102 (2019).
[39]S. R. Matthews, Y. J. Hwang, M. G. McCord, and M. A. Bourham, J. Appl. Polym. Sci. **94**, 2383 (2004).
[40]H. Puliyalil and U. Cvelbar, Nanomaterials **6**, 108 (2016).
[41]J. A. Murdzek and S. M. George, "Thermal atomic layer etching of amorphous and crystalline hafnium oxide, zirconium oxide, and hafnium zirconium oxide," *Proceedings of 2019 International Symposium on VLSI Technology, Systems and Application (VLSI-TSA)*, Hsinchu, Taiwan, *April 22–25, 2019* (IEEE, New York, 2019).
[42]J. W. Elam, M. D. Groner, and S. M. George, Rev. Sci. Instrum. **73**, 2981 (2002).
[43]R. D. Clark, S. Aoyama, S. Consiglio, G. Nakamura, and G. Leusink, ECS Trans. **35**, 815 (2011).
[44]S. Consiglio, R. D. Clark, E. Bersch, J. D. LaRose, I. Wells, K. Tapily, G. J. Leusink, and A. C. Diebold, ECS Trans. **41**, 89 (2011).
[45]K. Tapily, S. Consiglio, R. D. Clark, R. Vasic, E. Bersch, J. Jordan-Sweet, I. Wells, G. J. Leusink, and A. C. Diebold, ECS Trans. **45**, 411 (2012).
[46]R. Vasić *et al.*, J. Appl. Phys. **113**, 234101 (2013).
[47]"ZrO_2 XRD," in *Joint Committee for Powder Diffraction Standards, Powder Diffraction File No. 88-1007* (JCPDS International Center for Diffraction Data, Swarthmore, PA, 1998).
[48]"HfO_2 XRD," in *Joint Committee for Powder Diffraction Standards, Powder Diffraction File No. 78-0049* (JCPDS International Center for Diffraction Data, Swarthmore, PA, 1998).
[49]E. A. Scott *et al.*, Appl. Phys. Lett. **113**, 192901 (2018).
[50]T. Shiraishi *et al.*, Mater. Sci. Semicond. Process. **70**, 239 (2017).
[51]P. Kofstad and D. J. Ruzicka, J. Electrochem. Soc. **110**, 181 (1963).
[52]T. Kubo and T. Egawa, Semicond. Sci. Technol. **32**, 125016 (2017).
[53]K. Tse, D. Liu, K. Xiong, and J. Robertson, Microelectron. Eng. **84**, 2028 (2007).
[54]A. M. Cano, A. E. Marquardt, J. W. DuMont, and S. M. George, J. Phys. Chem. C **123**, 10346 (2019).
[55]HSC Chemistry, *HSC Chemistry 5.1* (Outokumpu Research Oy, Pori).
[56]H. F. Winters and J. W. Coburn, Appl. Phys. Lett. **34**, 70 (1979).
[57]J. F. Veyan, M. D. Halls, S. Rangan, D. Aureau, X. M. Yan, and Y. J. Chabal, J. Appl. Phys. **108**, 114914 (2010).